

# Ab initio study of highly tunable charge transfer in $\beta$ -RuCl<sub>3</sub>/graphene heterostructures

Aleksandar Razpopov<sup>1,\*</sup> and Roser Valentí<sup>1,†</sup>

<sup>1</sup>Institut für Theoretische Physik, Goethe-Universität Frankfurt, 60438 Frankfurt am Main, Germany

(Dated: June 13, 2024)

Heterostructures of graphene in proximity to magnetic insulators open the possibility to investigate exotic states emerging from the interplay of magnetism, strain and charge transfer between the layers. Recent reports on the growth of self-integrated atomic wires of  $\beta$ -RuCl<sub>3</sub> on graphite suggest these materials as versatile candidates to investigate these effects. Here we present detailed first principles calculations on the charge transfer and electronic structure of  $\beta$ -RuCl<sub>3</sub>/heterostructures and provide a comparison with the work function analysis of the related honeycomb family members  $\alpha$ -RuX<sub>3</sub> (X = Cl, Br, I). We find that proximity of the two layers leads to a hole-doped graphene and electron-doped RuX<sub>3</sub> in all cases, which is sensitively dependent on the distance between the two layers. Furthermore, strain effects due to lattice mismatch control the magnetization which itself has a strong effect on the charge transfer. Charge accumulation in  $\beta$ -RuCl<sub>3</sub> strongly drops away from the chain making such heterostructures suitable candidates for sharp interfacial junctions in graphene-based devices.

*Introduction.*- Graphene-based van der Waals (vdW) heterostructures reveal a variety of novel phenomena emerging from a notable modification of the electronic properties of their layer constituents due to proximity effects [1–10]. Some examples are heterostructures of graphene with several dichalcogenides like MoS<sub>2</sub>, WS<sub>2</sub>, and MoSe<sub>2</sub> with highly enhanced properties like ON/OFF current ratio in field effect transistors [3, 4], photoresponsivity [5, 6], capacitance [7–9], or thermoelectricity [10]. Such heterostructures are also desirable for possible technological applications as supercapacitors [7], photodetectors [11] and solid state lasers [12].

In recent years, heterostructures of graphene in proximity to magnetic insulators have gained increasing attention due to the possibility to investigate new states resulting from the interplay between charge transfer, strain and magnetism in the heterostructures. For instance, Ref. [13] reported hole-doping in graphene when placed in proximity to the magnetic insulators CrX<sub>3</sub> (X = Cl, Br, I), and found that the charge transfer from graphene to CrX<sub>3</sub> could be altered upon changing the magnetic states of the nearest magnetic insulator layer. Also, heterostructures of graphene with the Kitaev candidate material  $\alpha$ -RuCl<sub>3</sub> have been intensively investigated [14–22]. These studies find a significant charge transfer from graphene to  $\alpha$ -RuCl<sub>3</sub>, larger than in the CrI<sub>3</sub>/gr (graphene) heterostructure, giving rise to a van der Waals heterostructure that has higher conductivity than graphene. This charge transfer modifies the electronic properties of both materials and is influenced by the magnetism in  $\alpha$ -RuCl<sub>3</sub>, as evidenced by the observation of anomalous quantum oscillations near the magnetic ordering temperature of  $\alpha$ -RuCl<sub>3</sub>, that have been interpreted within a Kitaev-Kondo lattice model [23].

Motivated by this versatility of phases in heterostructures of graphene in proximity to magnetic insulators and in the search for systems where charge transfer could be considerable enough to modify the electronic prop-

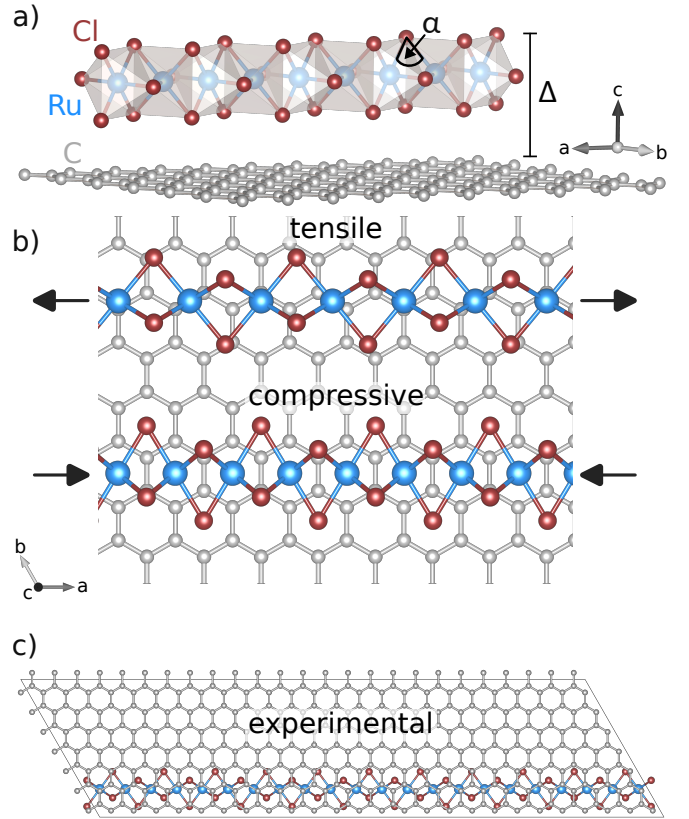


FIG. 1. a) Crystal structure of the heterostructure  $\beta$ -RuCl<sub>3</sub>/gr.  $\beta$ -RuCl<sub>3</sub> forms chains along the **a**-direction. Cl, Ru and C atoms are shown by dark red, light blue and grey balls, respectively. The chain height  $\Delta$  is defined as the z coordinate of the highest Cl atom, and the angle  $\alpha$  is between the Ru-Cl-Ru bond of the highest Cl atom. b) Cuts of  $5 \times 5$  and  $6 \times 6$  slabs of  $\beta$ -RuCl<sub>3</sub>/gr considered in this study, which are commensurate with 7.8% (tensile) and -13% (compressive) strains, respectively, as indicated by black arrows. c)  $7 \times 25$  slab of  $\beta$ -RuCl<sub>3</sub>/gr emulating the experimentally reported strained heterostructures [24].

erties of both layers, we explore here the charge transfer of heterostructures of graphene with RuBr<sub>3</sub> [25] and RuI<sub>3</sub> [26, 27], which are isostructural honeycomb van der Waals materials to the Kitaev candidate material  $\alpha$ -RuCl<sub>3</sub> [28–33], and we present detailed calculations of the heterostructure  $\beta$ -RuCl<sub>3</sub>/gr, where the chain-based  $\beta$ -RuCl<sub>3</sub> has recently been shown to grow as atomic-scale wires on graphite [24].

We proceed by first calculating the work functions for the various compounds within *ab initio* density functional theory (DFT). Relative comparisons to the work function of graphene provide an indication of the amount of expected charge transfer in the heterostructures. We then perform detailed calculations for  $\beta$ -RuCl<sub>3</sub>/gr by considering various strained structures adapted to the lattice mismatch between graphene and the magnetic insulator. Our main observations are that proximity of the two layers leads to a hole-doped graphene and electron-doped RuX<sub>3</sub> in all cases, which is sensitively dependent on the distance between the two layers. We further find that strain effects due to lattice mismatch, in first order, control the magnetization which itself has a strong effect on the charge transfer. Moreover, charge accumulation in  $\beta$ -RuCl<sub>3</sub> sharply drops away from the chain.

*Methods.*— In order to obtain the work functions of the various systems and to calculate the charge transfer and electronic properties of the heterostructure  $\beta$ -RuCl<sub>3</sub>/gr we use the projector augmented wave method [34] as implemented in the VASP simulation package [35] version 6.3.0. As exchange-correlation functional within DFT, we consider the generalized gradient approximation (GGA) [36] including the Coulomb corrections on the Ru 4d orbitals using the GGA+U scheme [37]. Additionally, van der Waals corrections are included via the DFT+D2 method of Grimme [38]. For structural relaxations we consider a  $6 \times 6 \times 1$  k-mesh, while for electronic property calculations we consider a  $12 \times 12 \times 1$  k-mesh that provides accurate results.

For the work function estimates we keep the crystal structures as provided by X-ray data [39] without further relaxing them. The work function  $W$  is given by [40]

$$W = E_{\text{vac}} - E_{\text{F}}, \quad (1)$$

where  $E_{\text{vac}}$  is the vacuum energy and  $E_{\text{F}}$  is the Fermi energy. The Fermi level is placed at the middle of the insulating gap. Note that for these calculations only monolayers of the corresponding materials were considered since previous DFT studies showed that the work function is primarily related to the surface properties [41].

The heterostructure  $\beta$ -RuCl<sub>3</sub>/gr is constructed from the experimental crystal structure of  $\beta$ -RuCl<sub>3</sub> [39] as shown in Fig. 1 a) top panel. For the slab calculations a void of  $d_{\text{layer}} = 20 \text{ \AA}$  is considered to ensure that the heterostructure is electronically isolated from the neighboring ones along the c-direction since the calculations assume periodic boundary conditions. As the graphene

layer has higher stiffness than  $\beta$ -RuCl<sub>3</sub>, its structure is fixed with  $d_{\text{C-C}} = 1.420 \text{ \AA}$  and only  $\beta$ -RuCl<sub>3</sub> is relaxed. The charge transfer is obtained via Bader analysis [42] of the optimized structure.

*Results.*— In Table I we present the calculated work functions  $W_{\text{DFT}}$  for the systems considered in this study. For  $\beta$ -RuCl<sub>3</sub> we also include the stress dependence of the work functions. For graphene and  $\alpha$ -RuCl<sub>3</sub> our calculated values are in excellent agreement with the  $W_{\text{exp}}$  values reported in earlier experimental works [43–45]. The

Materials	$ W_{\text{DFT}}[\text{eV}] $	$W_{\text{exp}}[\text{eV}]$
graphene	4.20	4.30 [43]
$\beta$ -RuCl <sub>3</sub> (-13%)	6.26	-
$\beta$ -RuCl <sub>3</sub>	6.04	-
$\beta$ -RuCl <sub>3</sub> (7.8%)	5.97	-
$\alpha$ -RuCl <sub>3</sub>	6.01	6.10 [44, 45]
RuBr <sub>3</sub>	5.64	-
RuI <sub>3</sub>	5.23	-

TABLE I. Calculated work functions of graphene, and monolayers of RuX<sub>3</sub> (X = Cl, Br, I) and  $\beta$ -RuCl<sub>3</sub>, under various stress conditions for the latter along the chain direction (compressive (-13%) and tensile (7.8%)), compare with Fig. 1). The calculated value for graphene agree with previous reported results including spin-orbit coupling (SOC) and considering HSE06 as exchange-correlation functional [46].

differences in work functions between graphene and the various RuX<sub>3</sub> monolayers already suggest that in all cases a graphene hole-doping is to be expected in the RuX<sub>3</sub>/gr heterostructures. The charge transfer is expected to increase in going from RuI<sub>3</sub> to RuCl<sub>3</sub>. Interestingly, while the work functions for  $\alpha$ - and  $\beta$ -RuCl<sub>3</sub> are similar, the effect of strain has an important impact on the resulting work function of  $\beta$ -RuCl<sub>3</sub> which increases under compressive strain and decreases under tensile strain. This effect is less remarkable in  $\alpha$ -RuCl<sub>3</sub> [16]. The above results suggest that  $\beta$ -RuCl<sub>3</sub>/gr under various conditions of strain may be a promising candidate to achieve considerable charge transfer, and therefore we concentrate in what follows on analyzing its electronic properties.

In order to simulate a strained heterostructure one needs to consider slabs that are commensurate with the chosen strain. The smaller the strain values, the larger the corresponding slabs that need to be considered. Balancing between numerical feasibility and complexity, we start with  $5 \times 5$  and  $6 \times 6$  slabs which allow to describe  $\beta$ -RuCl<sub>3</sub>/gr with  $\beta$ -RuCl<sub>3</sub> under 7.8% (tensile) and -13.0% (compressive) strain, respectively (see Fig. 1 b)). We first obtain geometrically optimized slab structures of  $\beta$ -RuCl<sub>3</sub>/gr (see SI for details) for these two extreme strained cases, and we then consider slab structures that are commensurate with the strain achieved in recent experiments [24, 47] (compressive, (-1.8%)) (Fig. 1 c)). All the reported values of strain are measured with respect to bulk  $\beta$ -RuCl<sub>3</sub> lattice parameters. Two different initial magnetic configurations of Ru chains were also consid-

ered for the relaxation of the slabs: ferromagnetic (FM) and antiferromagnetic (AFM) (see Fig. S2 in SI). In a second step we analyze the electronic properties and charge transfer for the various slabs.

Starting with the 7.8% tensile configuration, the initial geometry of  $\beta$ -RuCl<sub>3</sub> consists of a uniform Ru-Ru chain, where the Ru atoms are centered above a C atom and in-between two C atoms of graphene in an alternating fashion (Fig. 1 b)). After the structural relaxation within GGA+U,  $U - J = U_{\text{eff}} = 3.0$  eV and a FM configuration of Ru, the final configuration switches from FM to double-AFM (dAFM), with two-up and two-down magnetic moments along the Ru chain (see Fig. S2 in SI). This relaxed structure displays three different Ru-Ru distances:  $d_{\text{Ru-Ru}}^{(1)} = 3.138$  Å,  $d_{\text{Ru-Ru}}^{(2)} = 3.065$  Å, and  $d_{\text{Ru-Ru}}^{(3)} = 2.949$  Å. The amount of dimerization of the chain, given by the ratio of the longest to shortest Ru-Ru bond-distance, is  $\approx 6\%$ . Note that this configuration shows a weaker chain dimerization than the reported dimerized structure of bulk  $\beta$ -RuCl<sub>3</sub> of  $\approx 13\%$  at low temperatures [48]. The associated Ru-Cl-Ru angles along the chain  $\alpha$  (Fig. 1 a)) get modified as well, introducing a slight non-linearity in the Ru chains with the angles lying between  $0.3^\circ - 0.7^\circ$  compared to a perfectly linear chain of Ru atoms. We also performed structural relaxations starting with an AFM configuration and we reached the same optimized structure and magnetic configuration as described above, showing that the final relaxed geometry is not dependent on the initial magnetic configuration.

Total energy calculations of the optimized structures show that FM and dAFM configurations are energetically highly competing states. For further analysis of the optimized structure, as shown below, we will consider therefore, for simplicity, the optimized strained structure with Ru in a FM configuration.

Fig. 2 a) displays the calculated electronic band structure and atom resolved density of states (DOS) within GGA+U for the 7.8% strained  $\beta$ -RuCl<sub>3</sub>/gr heterostructure. Note that the  $5 \times 5$ -graphene's **K** point folds back on itself [49]. We observe that the Dirac point shifts by about 0.50 eV above the Fermi energy  $E_F$  compared to pure graphene, indicating hole doping (charge depletion) in the graphene layer. This shift of the Dirac point is consistent with a positive value of the calculated difference in work functions ( $W_{\text{RuCl}_3} - W_{\text{Graphene}} \approx 2$  eV).

In contrast to the Mott insulating behavior of bulk  $\beta$ -RuCl<sub>3</sub> [24], the heterostructure  $\beta$ -RuCl<sub>3</sub>/gr undergoes an insulator to metal transition due to the chemical shift. The electronic weights at the Fermi level are mostly of Ru  $d$  orbitals hybridizing with Cl and C  $p$  orbitals (see DOS in Fig. 2 a)). The Ru flat bands pinned near the Fermi level are a consequence of the tensile strain on  $\beta$ -RuCl<sub>3</sub> which drives the chain towards an atomic limit with localized bands.

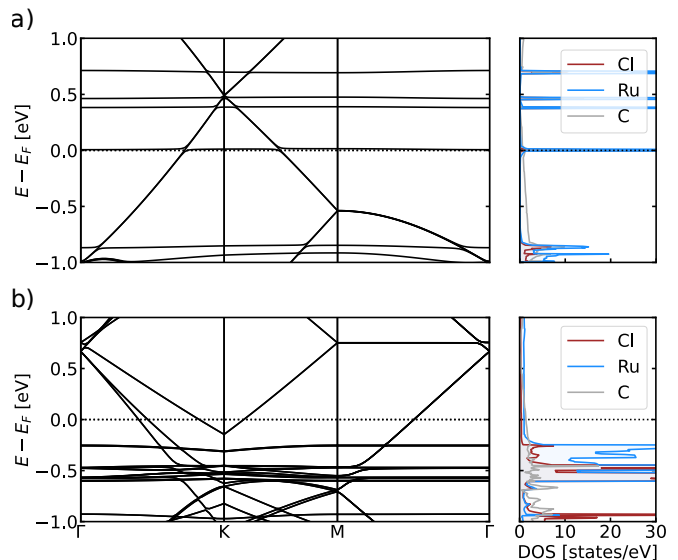


FIG. 2. Band structure and atom-resolved DOS of a)  $\beta$ -RuCl<sub>3</sub>/gr under 7.8% tensile strain with FM ordered moments on the Ru sites. The Dirac point of pristine graphene at the **K** point is shifted  $\approx 0.50$  eV above the Fermi level. b)  $\beta$ -RuCl<sub>3</sub>/gr under -13% compressive strain. The Dirac point of graphene at the  $\Gamma$  point is shifted by  $\approx 0.65$  eV above the Fermi surface. In both cases there is charge transfer from graphene to the  $\beta$ -RuCl<sub>3</sub> chain. The results were obtained with GGA+U, with  $U - J = U_{\text{eff}} = 3.0$  eV.

Using Bader analysis [42] we compute the charge transfer per formula unit between  $\beta$ -RuCl<sub>3</sub> and graphene.  $\beta$ -RuCl<sub>3</sub> is electron-doped with  $\delta\rho_{\text{RuCl}_3} = 0.085$  e/f.u. and graphene hole-doped with  $\delta\rho_C = -0.007$  e/C. These values have been also confirmed for AFM and dAFM configurations of Ru, where we observed negligible differences of less than 5% due to numerical approximations. We also studied the dependence of the charge transfer on the presence of Ru magnetic moments by performing non-magnetic calculations and found a significant increase of the charge transfer by  $\approx 37\%$ , compared to the magnetic case. This result indicates a strong correlation between magnetism and charge transfer in this system.

Next, we investigate  $\beta$ -RuCl<sub>3</sub>/gr under compressive strain (Fig. 2 b)) by considering a  $6 \times 6$  slab where initially Ru atoms are positioned at the center of the carbon honeycomb in graphene. Structural relaxation with both, FM and AFM initial magnetic configurations for Ru lead to the same relaxed non-magnetic solution where  $d_{\text{Ru-Ru}} = 2.459$  Å forming regular linear chains (Fig. 1 b)), in contrast to the tensile heterostructure above. The reduced Ru-Ru distance corresponds to 13% compressive strain compared to the bulk undimerized structure with  $d_{\text{Ru-Ru}}^{\text{Bulk}} = 2.861$  Å. The height of the  $\beta$ -RuCl<sub>3</sub> to graphene,  $\Delta$  (Fig. 1 a)), increases from 6.5 Å to 6.7 Å going from tensile to compressive strain as a consequence of the shortening of the Ru-Ru distance that increases the angle  $\alpha$  changing the value of the height. This height

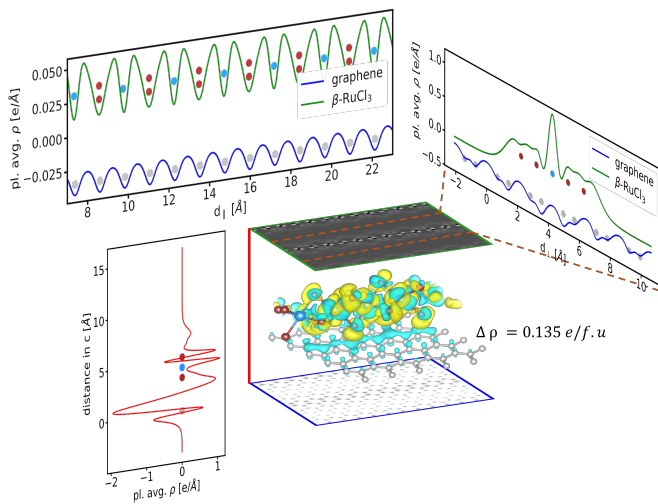


FIG. 3. Spatial charge redistribution in the (-13%) compressive strained  $\beta$ -RuCl<sub>3</sub>/gr,  $\Delta\rho = \Delta\rho_{\text{RuCl}_3/\text{gr}} - \Delta\rho_{\text{RuCl}_3} - \Delta\rho_{\text{gr}}$ . The figure shows in the top panels a two-dimensional projection of the planer-average charge density (pl. avg.  $\Delta\rho$ ) along the parallel ( $d_{\parallel}$ ) and perpendicular ( $d_{\perp}$ ) chain directions in the  $ab$  plane. Dots in grey, light blue and dark red symbolize the position of the C, Ru and Cl atoms. The green and blue curves display the 2D projection of pl. avg.  $\Delta\rho$  within the  $\beta$ -RuCl<sub>3</sub> and graphene layers, respectively. The central panel shows a three-dimensional view of  $\Delta\rho$ . In the bottom left panel the total charge redistribution along  $c$  is shown as a red curve. The planer-average charge values are multiplied by a factor of 1000.

profile of the relaxed heterostructures is close to the obtained from experiment [24].

In Fig. 2 b) we show the calculated band structure and DOS for this case. In contrast to the tensile case, no Ru states are pinned near the Fermi level. The reason for that is the short Ru-Ru distance due to the compressed chain structure inducing Ru-Ru bonding-antibonding band splittings located at -0.5eV and 2.5eV respectively (see Fig. S6 in SI). The Dirac point of pristine graphene is folded back to the  $\Gamma$  point of the heterostructure due to the choice of the super-cell [49] and shifted  $\approx 0.65$  eV above the Fermi energy. This indicates a higher charge transfer compared to the tensile strain. This result is in agreement to the trends found in the  $W_{\text{DFT}}$  differences (Table I), that suggest an increase of charge transfer from tensile to compressive strain.

The Bader analysis [42] for the compressed  $\beta$ -RuCl<sub>3</sub>/gr confirms that the charge transfer is strongly enhanced compared to the tensile strained heterostructure. We observe electron doping in  $\beta$ -RuCl<sub>3</sub>,  $\delta\rho_{\text{RuCl}_3} = 0.134$  e/f.u., which is 37% larger than in the tensile case, and hole doping in graphene with  $\delta\rho_{\text{C}} = -0.012$  e/C. This amount of charge transfer coincides with the non-magnetic estimates for the tensile strained heterostructure and corroborates the observation of a strong correlation between the absolute value of the Ru magnetic

moment and the charge transfer.

Fig. 3 displays the spatial charge redistribution along the three directions for the compressive strained  $\beta$ -RuCl<sub>3</sub>/gr (results for the tensile strained heterostructure are shown in SI). Along the  $c$ -direction we observe a strong charge depletion (negative  $\Delta\rho$ ) at the graphene layer and charge accumulation (positive  $\Delta\rho$ ) at the  $\beta$ -RuCl<sub>3</sub> layer (Fig. 3 bottom left panel). Along the chain direction ( $d_{\parallel}$ , Fig. 3 top left panel) the charge distribution follows a uniform pattern, while in the direction perpendicular to it ( $d_{\perp}$ , Fig. 3 top right panel), the charge accumulation at the atomic wire sharply decays and goes to zero within a few Angstroms away from the chain, similar to what has been observed in  $\alpha$ -RuCl<sub>3</sub> stripes on graphene [20]. We further investigated the dependence of the relative orientation of the  $\beta$ -RuCl<sub>3</sub> chains to graphene keeping the height constant, but we didn't find any significant changes in the charge transfer (see SI).

In order to estimate whether the above considered heterostructures are realizable we calculate the formation enthalpy  $\Delta H$  defined as

$$\Delta H = E(AB) - E(A) - E(B), \quad (2)$$

where  $E(AB)$  is the energy of the  $\beta$ -RuCl<sub>3</sub>/gr heterostructure, and  $E(A)$  and  $E(B)$  are the energies of the subsystems A (graphene) and B ( $\beta$ -RuCl<sub>3</sub>-chain). For the tensile strained  $\beta$ -RuCl<sub>3</sub>/gr,  $\Delta H_T = -0.230$  meV/f.u. and for the compressive strained  $\beta$ -RuCl<sub>3</sub>/gr,  $\Delta H_C = -0.320$  meV/f.u. From this analysis we conclude that both strained heterostructures are stable and could be realized in experiments.

We proceed now with the study of a slab of  $\beta$ -RuCl<sub>3</sub>/gr (see Fig. 1 c)) corresponding to recently reported strained heterostructures [24, 47] showing  $\approx 2\%$  compressive strain. Since the analysis performed so far in the  $5 \times 5$  and  $6 \times 6$  slabs suggests no significant dependence on the relative orientation of the chains and graphene, we do not relax the full heterostructure, what would lead to unsustainable heavy calculations due to the large number of atoms in the slab. Instead, we select for the height of the chain  $\Delta$  (Fig. 1 a)) a value close to the estimates obtained for the above analyzed heterostructures and we consider Ru magnetic moments initially in a FM configuration. We find via Bader analysis a charge transfer of  $\delta\rho_{\text{RuCl}_3} = 0.113$  e/f.u. and  $\delta\rho_{\text{C}} = -0.007$  e/C. To compare the results of the three heterostructures we plot in Fig. 4 a) the dependence of the charge transfer on the average magnetic moment on the Ru sites. We observe a direct relation between a decrease of charge with an increase of magnetic moment. Actually, the value of the charge transfer for all three cases in non-magnetic calculations is the same. These results suggest that strain in first order controls the magnetization which itself has a strong effect on the charge transfer. Besides strain, changing the height  $\Delta$  offers as well a possibility to modify the charge transfer. Increasing the layer

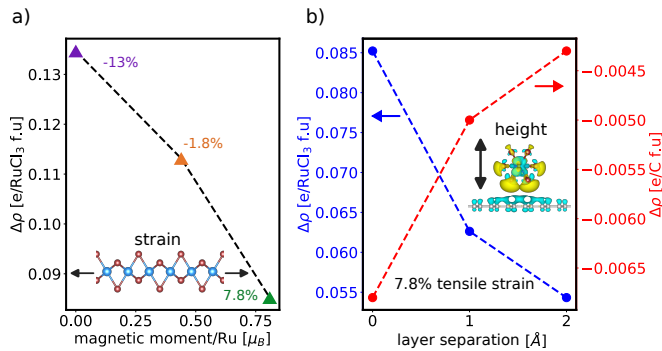


FIG. 4. Possible charge-transfer tuning parameters. a) Dependence between the magnetic moment and the charge transfer. Each colored data point refers to a different heretostucture setting: purple to tensile strain, orange to experimental strain and green to compressive strain. The strain symbolizes a way to control the magnetic moment. b) Charge transfer in the tensile strained structure as a function of the manually controlled layer separation distance.

separation between  $\beta$ -RuCl<sub>3</sub> and graphene leads to decreasing charge transfer. In Fig. 4 b) we show this dependence for the tensile heterostructure. This behavior is to be expected and has been observed in other van der Waals heterostructures [50]. Experimentally, it is also possible to control the distance between two atomic wires as shown by the synthesis technique of  $\beta$ -RuCl<sub>3</sub> used in Ref. [24]. We therefore analyzed the charge transfer as a function of interchain distance but no significant changes were observed as can be already preempted by the fact that charge accumulation perpendicular to the  $\beta$ -RuCl<sub>3</sub> chains sharply drops at the edges (see Fig. 3 top right panel).

*Conclusions.*- We have investigated via first principles calculations, the charge transfer and electronic properties of heterostructures of graphene with the honeycomb-based  $\alpha$ -RuX<sub>3</sub>, (X = Cl, Br, I) and chain-based  $\beta$ -RuCl<sub>3</sub> by calculating work functions and by performing slab simulations of the recently reported  $\beta$ -RuCl<sub>3</sub>/gr heterostructure [24]. Our calculations on three exemplary heterostructures of  $\beta$ -RuCl<sub>3</sub>/gr including different degrees of tensile and compressive strain showed that proximity of the two layers leads to a hole-doped graphene and electron-doped RuX<sub>3</sub> in all cases, which is sensitively dependent on the distance between the two layers. Furthermore, strain effects due to lattice mismatch, control the magnetization which itself has a strong effect on the charge transfer, and charge accumulation in  $\beta$ -RuCl<sub>3</sub> sharply drops away from the chain what opens the possibility for device development.

*Acknowledgements.*- The authors are grateful to S. Biswas, T. Asaba, K. Burch, and E. Henriksen for valuable discussions and gratefully acknowledge support by the Deutsche Forschungsgemeinschaft (DFG, German Research Foundation) for funding through Project No.

509751747 (VA 117/23-1) and TRR 288 — 422213477 (project A05).

\* [razpopov@itp.uni-frankfurt.de](mailto:razpopov@itp.uni-frankfurt.de)

† [valenti@itp.uni-frankfurt.de](mailto:valenti@itp.uni-frankfurt.de)

- [1] A. K. Geim and I. V. Grigorieva, Van der waals heterostructures, *Nature* **499**, 419 (2013), perspective.
- [2] K. S. Novoselov, A. Mishchenko, A. Carvalho, and A. H. Castro Neto, 2d materials and van der waals heterostructures, *Science* **353** (2016).
- [3] W. J. Yu, Z. Li, H. Zhou, Y. Chen, Y. Wang, Y. Huang, and X. Duan, Vertically stacked multi-heterostructures of layered materials for logic transistors and complementary inverters, *Nature materials* **12**, 246 (2013).
- [4] L. Britnell, R. Gorbachev, R. Jalil, B. Belle, F. Schedin, A. Mishchenko, T. Georgiou, M. Katsnelson, L. Eaves, S. Morozov, *et al.*, Field-effect tunneling transistor based on vertical graphene heterostructures, *Science* **335**, 947 (2012).
- [5] W. Zhang, C.-P. Chuu, J.-K. Huang, C.-H. Chen, M.-L. Tsai, Y.-H. Chang, C.-T. Liang, Y.-Z. Chen, Y.-L. Chueh, J.-H. He, *et al.*, Ultrahigh-gain photodetectors based on atomically thin graphene-mos2 heterostructures, *Scientific reports* **4**, 3826 (2014).
- [6] J. D. Mehew, S. Unal, E. Torres Alonso, G. F. Jones, S. Fadhil Ramadhan, M. F. Craciun, and S. Russo, Fast and highly sensitive ionic-polymer-gated ws2-graphene photodetectors, *Advanced Materials* **29**, 1700222 (2017).
- [7] M. Saraf, K. Natarajan, and S. M. Mobin, Emerging robust heterostructure of mos2-rgo for high-performance supercapacitors, *ACS applied materials & interfaces* **10**, 16588 (2018).
- [8] S. Ratha and C. S. Rout, Supercapacitor electrodes based on layered tungsten disulfide-reduced graphene oxide hybrids synthesized by a facile hydrothermal method, *ACS applied materials & interfaces* **5**, 11427 (2013).
- [9] B. Kirubasankar, S. Vijayan, and S. Angaiah, Sonochemical synthesis of a 2d-2d mose 2/graphene nanohybrid electrode material for asymmetric supercapacitors, *Sustainable Energy & Fuels* **3**, 467 (2019).
- [10] H. Sadeghi, S. Sangtarash, and C. J. Lambert, Cross-plane enhanced thermoelectricity and phonon suppression in graphene/mos2 van der waals heterostructures, *2D Materials* **4**, 015012 (2016).
- [11] A. S. Aji, P. Solís-Fernández, H. G. Ji, K. Fukuda, and H. Ago, High mobility ws2 transistors realized by multilayer graphene electrodes and application to high responsivity flexible photodetectors, *Advanced Functional Materials* **27**, 1703448 (2017).
- [12] G. Zhao, J. Hou, Y. Wu, J. He, and X. Hao, Preparation of 2d mos2/graphene heterostructure through a monolayer intercalation method and its application as an optical modulator in pulsed laser generation, *Advanced Optical Materials* **3**, 937 (2015).
- [13] C.-C. Tseng, T. Song, Q. Jiang, Z. Lin, C. Wang, J. Suh, K. Watanabe, T. Taniguchi, M. A. McGuire, D. Xiao, *et al.*, Gate-tunable proximity effects in graphene on layered magnetic insulators, *Nano Letters* **22**, 8495 (2022).
- [14] B. Zhou, J. Balgley, P. Lampen-Kelley, J.-Q. Yan, D. G. Mandrus, and E. A. Henriksen, Evidence for charge

- transfer and proximate magnetism in graphene- $\alpha$ -rucl<sub>3</sub> heterostructures, *Phys. Rev. B* **100**, 165426 (2019).
- [15] S. Mashhadi, Y. Kim, J. Kim, D. Weber, T. Taniguchi, K. Watanabe, N. Park, B. Lotsch, J. H. Smet, M. Burghard, and K. Kern, Spin-split band hybridization in graphene proximitized with  $\alpha$ -rucl<sub>3</sub> nanosheets, *Nano Letters* **19**, 4659 (2019), pMID: 31241971.
- [16] S. Biswas, Y. Li, S. M. Winter, J. Knolle, and R. Valentí, Electronic properties of  $\alpha$ -rucl<sub>3</sub> in proximity to graphene, *Phys. Rev. Lett.* **123**, 237201 (2019).
- [17] D. J. Rizzo, B. S. Jessen, Z. Sun, F. L. Ruta, J. Zhang, J.-Q. Yan, L. Xian, A. S. McLeod, M. E. Berkowitz, K. Watanabe, *et al.*, Charge-transfer plasmon polaritons at graphene/ $\alpha$ -rucl<sub>3</sub> interfaces, *Nano letters* **20**, 8438 (2020).
- [18] E. Gerber, Y. Yao, T. A. Arias, and E.-A. Kim, Ab initio mismatched interface theory of graphene on  $\alpha$ -rucl<sub>3</sub>: Doping and magnetism, *Phys. Rev. Lett.* **124**, 106804 (2020).
- [19] Y. Wang, J. Balgley, E. Gerber, M. Gray, N. Kumar, X. Lu, J.-Q. Yan, A. Fereidouni, R. Basnet, S. J. Yun, *et al.*, Modulation doping via a two-dimensional atomic crystalline acceptor, *Nano letters* **20**, 8446 (2020).
- [20] J. Balgley, J. Butler, S. Biswas, Z. Ge, S. Lagasse, T. Taniguchi, K. Watanabe, M. Cothrine, D. G. Mandrus, J. Velasco Jr, *et al.*, Ultrasharp lateral p-n junctions in modulation-doped graphene, *Nano Letters* **22**, 4124 (2022).
- [21] B. Yang, Y. M. Goh, S. H. Sung, G. Ye, S. Biswas, D. A. S. Kaib, R. Dhakal, S. Yan, C. Li, S. Jiang, F. Chen, H. Lei, R. He, R. Valentí, S. M. Winter, R. Hovden, and A. W. Tsen, Magnetic anisotropy reversal driven by structural symmetry-breaking in monolayer  $\alpha$ -rucl<sub>3</sub>, *Nature Materials* **22**, 50–57 (2022).
- [22] A. Rossi, C. Johnson, J. Balgley, J. C. Thomas, L. Francaviglia, R. Dettori, A. K. Schmid, K. Watanabe, T. Taniguchi, M. Cothrine, *et al.*, Direct visualization of the charge transfer in a graphene/ $\alpha$ -rucl<sub>3</sub> heterostructure via angle-resolved photoemission spectroscopy, *Nano Letters* **23**, 8000 (2023).
- [23] V. Leeb, K. Polyudov, S. Mashhadi, S. Biswas, R. Valentí, M. Burghard, and J. Knolle, Anomalous quantum oscillations in a heterostructure of graphene on a proximate quantum spin liquid, *Physical Review Letters* **126**, 097201 (2021).
- [24] T. Asaba, L. Peng, T. Ono, S. Akutagawa, I. Tanaka, H. Murayama, S. Suetsugu, A. Razpopov, Y. Kasahara, T. Terashima, Y. Kohsaka, T. Shibauchi, M. Ichikawa, R. Valentí, S. ichi Sasa, and Y. Matsuda, Growth of self-integrated atomic quantum wires and junctions of a mott semiconductor, *Science Advances* **9**, eabq5561 (2023).
- [25] Y. Imai, K. Nawa, Y. Shimizu, W. Yamada, H. Fujihara, T. Aoyama, R. Takahashi, D. Okuyama, T. Ohashi, M. Hagihala, *et al.*, Zigzag magnetic order in the kitaev spin-liquid candidate material rucl<sub>3</sub> with a honeycomb lattice, *Physical Review B* **105**, L041112 (2022).
- [26] K. Nawa, Y. Imai, Y. Yamaji, H. Fujihara, W. Yamada, R. Takahashi, T. Hiraoka, M. Hagihala, S. Torii, T. Aoyama, *et al.*, Strongly electron-correlated semimetal rui<sub>3</sub> with a layered honeycomb structure, *Journal of the Physical Society of Japan* **90**, 123703 (2021).
- [27] D. Ni, X. Gui, K. M. Powderly, and R. J. Cava, Honeycomb-structure rui<sub>3</sub>, a new quantum material related to  $\alpha$ -rucl<sub>3</sub>, *Advanced Materials* **34**, 2106831 (2022).
- [28] S. M. Winter, A. A. Tsirlin, M. Daghofer, J. van den Brink, Y. Singh, P. Gegenwart, and R. Valentí, Models and materials for generalized kitaev magnetism, *Journal of Physics: Condensed Matter* **29**, 493002 (2017).
- [29] Y. Motome and J. Nasu, Hunting majorana fermions in kitaev magnets, *Journal of the Physical Society of Japan* **89**, 012002 (2020).
- [30] D. A. Kaib, K. Riedl, A. Razpopov, Y. Li, S. Backes, I. I. Mazin, and R. Valentí, Electronic and magnetic properties of the rux<sub>3</sub> (x= cl, br, i) family: two siblings—and a cousin?, *npj Quantum Materials* **7**, 75 (2022).
- [31] S. Kim, B. Yuan, and Y.-J. Kim,  $\alpha$ -rucl<sub>3</sub> and other kitaev materials, *APL Materials* **10** (2022).
- [32] S. Trebst and C. Hickey, Kitaev materials, *Physics Reports* **950**, 1 (2022).
- [33] Y. Ahn, X. Guo, S. Son, Z. Sun, and L. Zhao, Progress and prospects in two-dimensional magnetism of van der waals materials, *Progress in Quantum Electronics* , 100498 (2024).
- [34] P. E. Blöchl, Projector augmented-wave method, *Phys. Rev. B* **50**, 17953 (1994).
- [35] G. Kresse and J. Hafner, Ab initio molecular dynamics for liquid metals, *Phys. Rev. B* **47**, 558 (1993).
- [36] J. P. Perdew, K. Burke, and M. Ernzerhof, Generalized gradient approximation made simple, *Phys. Rev. Lett.* **77**, 3865 (1996).
- [37] S. L. Dudarev, G. A. Botton, S. Y. Savrasov, C. J. Humphreys, and A. P. Sutton, Electron-energy-loss spectra and the structural stability of nickel oxide: An lsd<sub>a</sub>+u study, *Phys. Rev. B* **57**, 1505 (1998).
- [38] S. Grimme, Semiempirical gga-type density functional constructed with a long-range dispersion correction, *Journal of Physics and Chemistry of Solids* **27**, 1787 (2006).
- [39] J. M. Fletcher, W. E. Gardner, A. C. Fox, and G. Topping, X-ray, infrared, and magnetic studies of  $\alpha$ - and  $\beta$ -ruthenium trichloride, *J. Chem. Soc. A* , 1038 (1967).
- [40] A. Kahn, Fermi level, work function and vacuum level, *Materials Horizons* **3**, 7 (2016).
- [41] H.-g. Kim and H. J. Choi, Thickness dependence of work function, ionization energy, and electron affinity of mo and w dichalcogenides from dft and gw calculations, *Phys. Rev. B* **103**, 085404 (2021).
- [42] G. Henkelman, A. Arnaldsson, and H. Jónsson, A fast and robust algorithm for bader decomposition of charge density, *Computational Materials Science* **36**, 354 (2006).
- [43] E. Rut'kov, E. Afanas'eva, and N. Gall, Graphene and graphite work function depending on layer number on re, *Diamond and Related Materials* **101**, 107576 (2020).
- [44] I. Pollini, Electronic properties of the narrow-band material  $\alpha$ -rucl<sub>3</sub>, *Phys. Rev. B* **53**, 12769 (1996).
- [45] T. Klapproth, M. Grönke, S. Hampel, M. Knupfer, B. Büchner, A. Isaeva, T. Doert, and A. Koitzsch, Work function engineering of thin  $\alpha$ -rucl<sub>3</sub> by argon sputtering, *Advanced Materials Interfaces* **9**, 2200754 (2022).
- [46] J. Zhang, B. Zhao, T. Zhou, Y. Xue, C. Ma, and Z. Yang, Strong magnetization and chern insulators in compressed graphene/cr<sub>3</sub> van der waals heterostructures, *Physical Review B* **97**, 085401 (2018).
- [47] Private communication with Tomoya Asaba.
- [48] H. Hillebrecht, T. Ludwig, and G. Thiele, About trihalides with tii<sub>3</sub> chain structure: Proof of pair forming of cations in  $\beta$ -rucl<sub>3</sub> and rucl<sub>3</sub> by temperature dependent single crystal x-ray analyses, *Zeitschrift für anorganische und allgemeine Chemie* **630**, 2199 (2004).

- [49] Y.-C. Zhou, H.-L. Zhang, and W.-Q. Deng, A  $3n$  rule for the electronic properties of doped graphene, *Nanotechnology* **24**, 225705 (2013).
- [50] L. Crippa, H. Bae, P. Wunderlich, I. I. Mazin, B. Yan, G. Sangiovanni, T. Wehling, and R. Valentí, Heavy fermions vs doped mott physics in heterogeneous t-dichalcogenide bilayers, *Nature Communications* **15**, 1357 (2024).

## Supplementary Information:

### *Ab initio* study of highly tunable charge transfer in $\beta$ -RuCl<sub>3</sub>/graphene heterostructures

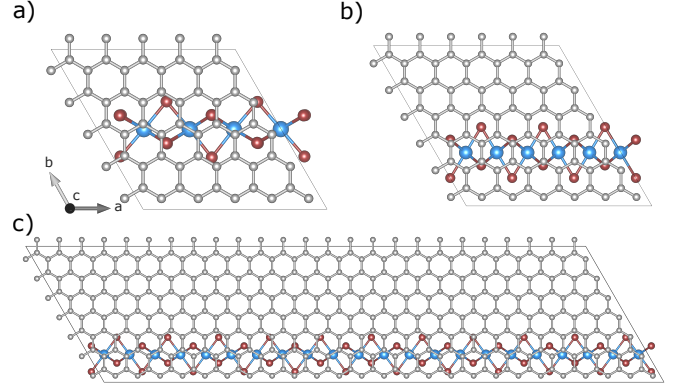
#### Supplementary Note 1: Work function

We calculate via *ab initio* density functional theory (DFT) the work function  $W$  for graphene and the RuX<sub>3</sub> family with X=Cl, Br, I and compare with the experimental values if they are available (see main text), as implemented in VASP [35]. The simulations are performed on a  $10 \times 10 \times 5$   $\Gamma$ -centered  $\mathbf{k}$ -mesh for  $\alpha$ -RuCl<sub>3</sub>, RuBr<sub>3</sub>, and RuI<sub>3</sub> and for  $\beta$ -RuCl<sub>3</sub> on a  $8 \times 1 \times 22$ . As exchange correlation functional we use GGA [36] and include the Coulomb corrections on the Ru 4d orbitals using the DFT+U scheme [37]. We set  $U_{\text{eff}} = 3.0, 2.5, 2.0,$  and  $1.5$  eV for  $\beta$ -RuCl<sub>3</sub>,  $\alpha$ -RuCl<sub>3</sub>, RuBr<sub>3</sub> and RuI<sub>3</sub> motivated by constrained random-phase approximation (cRPA) estimates [30], respectively. Spin orbit effects are taken into account. The basis set plane wave cut-off for the expansion is set to 600 eV in each calculation. For all systems the work function  $W$  has been checked with respect to the size of the void, where all values are given for a void of the size of  $2 \times \mathbf{c}$  lattice constant of the responding material.

#### Supplementary Note 2: Heterostructures calculations

Using DFT we optimize the heterostructure of  $\beta$ -RuCl<sub>3</sub>/gr for tensile (+7.8%) and compressive strain (-13%), where we keep the graphene layer fixed, as graphene has high stiffness. The tensile strain simulation is performed with a  $2 \times 1$ - $\beta$ -RuCl<sub>3</sub> chain on  $5 \times 5$  graphene layer. In the initial geometry the Ru atoms are centered alternating above a C atom and in between a C-C bond. The compressive strain heterostructure consists of a  $3 \times 1$   $\beta$ -RuCl<sub>3</sub> chain on  $6 \times 6$  graphene, where each Ru atom is initially set above the center of a honeycomb built by the C atoms. The initial geometry of each structure consists of uniform chain, the simulated unit cells are shown in Supplementary Fig. 1. The experimental strain (not relaxed) consists of  $11 \times 1$   $\beta$ -RuCl<sub>3</sub> chain on  $7 \times 25$  graphene. We include the Coulomb corrections on the Ru 4d orbitals using the DFT+U scheme [37], with  $U_{\text{eff}} = 3.0$  eV. The calculations are carried on a  $6 \times 6 \times 1$   $\mathbf{k}$ -grid for the compressive and tensile case, and on a  $1 \times 2 \times 1$   $\mathbf{k}$ -grid for the experimental strain with a basis set plane wave cut-off for the expansion is set to 600 eV. The graphene layer distance is set to  $d_{\text{layer}} = 20$  Å with C-C distance within the graphene layer of  $d_{\text{C-C}} = 1.420$  Å. This large layer distance  $d_{\text{layer}}$  ensures that the layer-layer interactions can be neglected and considered as a 2D system. The heterostructure is relaxed until the forces decrease down to  $10^{-3}$  eV/Å and energy convergence criterion of  $1 \times 10^{-6}$

eV.



Supplementary Figure 1. In panel **a**) we show the unit cell size used for the tensile strain, **b**) compressive unit cell size. In **c**) we show the unit cell used to simulate the experimental strain.

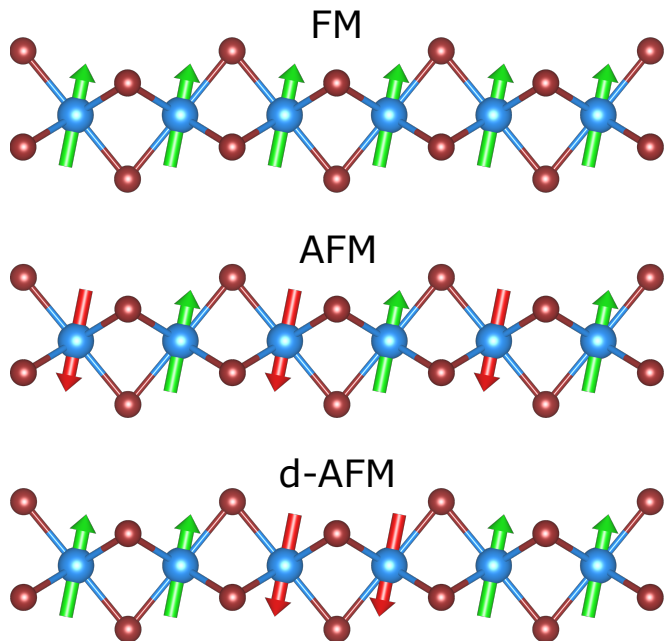
For each strain the structures are relaxed using ferromagnetic (FM), antiferromagnetic (AFM), and double-antiferromagnetic (dAFM) ordered magnetic, symbolized in Supplementary Fig. 2. We find that final structure does not depend on the magnetic order. Starting from the AFM state we obtain  $d_{\text{Ru-Ru}}^{(1)} = 3.137$  Å,  $d_{\text{Ru-Ru}}^{(2)} = 3.063$  Å, and  $d_{\text{Ru-Ru}}^{(3)} = 2.951$  Å. These values show very small deviation compared to the FM and dAFM state (see main text).

The electronic properties of the system are calculated in each relaxed structure with a more denser  $\mathbf{k}$ -grid of  $12 \times 12 \times 1$ . When comparing the total energy of each magnetic configuration, we find that FM state is energetically most favorable state, with 4 meV/f.u. lower compared to the dAFM order. The AFM state is the energetic highest state with 84 meV/f.u. above the dAFM solution.

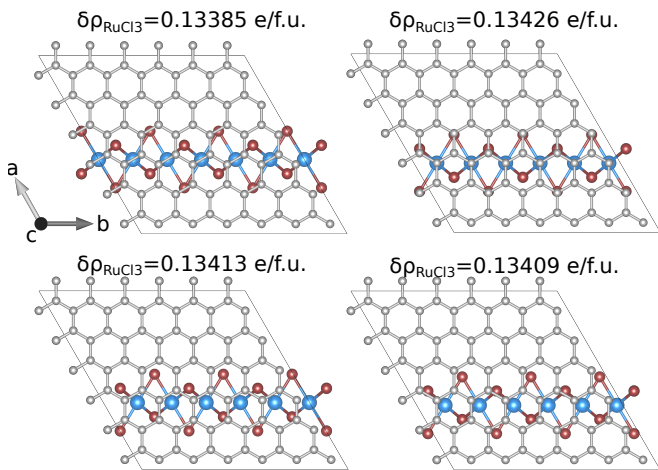
#### Supplementary Note 3: Geometry dependence

We study the dependence of the charge transfer and the relative orientation between the  $\beta$ -RuCl<sub>3</sub> atomic wire and the graphene layer. For this we considered four additional chain orientations in the compressed case, see Supplementary Fig. 3. Here, we keep the height  $\Delta$  from the first relaxed structure and shift manually the chain in the  $\mathbf{a-b}$  plane. Via Bader analysis [42] we computed the charge transfer for each case, the values in the  $\beta$ -RuCl<sub>3</sub> layer are noted in Supplementary Fig. 3. We observe negligible difference in the charge transfer.





Supplementary Figure 2. Different magnetic orders investigated during this study: ferromagnetic order (FM), antiferromagnetic (AFM), and double antiferromagnetic (d-AFM). The green up arrows symbolize the magnetic moment with spin up, and the red arrows the spin down.

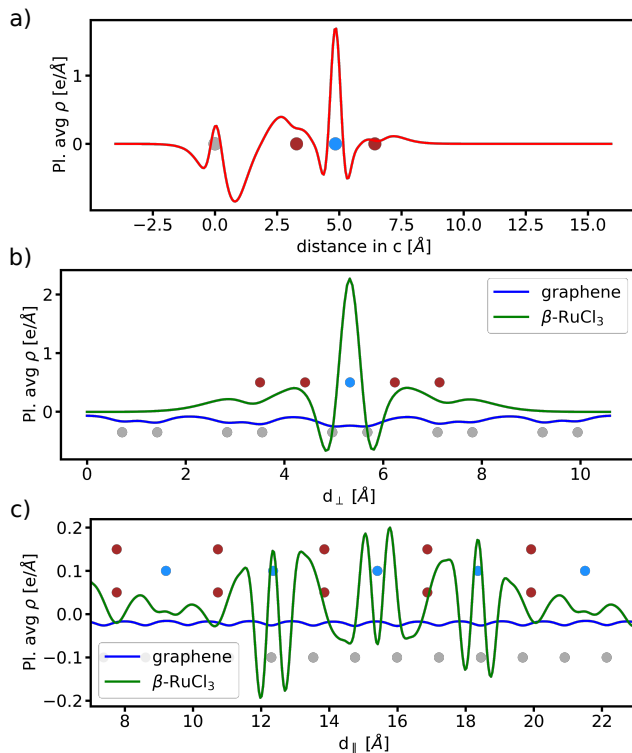


Supplementary Figure 3. Additional relative geometries that have been investigated in the compressive setting. Above each setting we note the charge transfer  $\delta\rho_{\text{RuCl}_3}$ .

#### Supplementary Note 4: Charge distribution tensile strain

In Supplementary Fig. 4 we show the average charge redistribution in each direction in the tensile structure (7.8%). We see very similar behavior for the charge along *c*-direction (Supplementary Fig. 4a) and perpendicular direction (Supplementary Fig. 4b)) like in the compressive strain (see main text). As in the compressive case the charge redistribution in the  $\beta$ -RuCl<sub>3</sub> atomic wire, shown

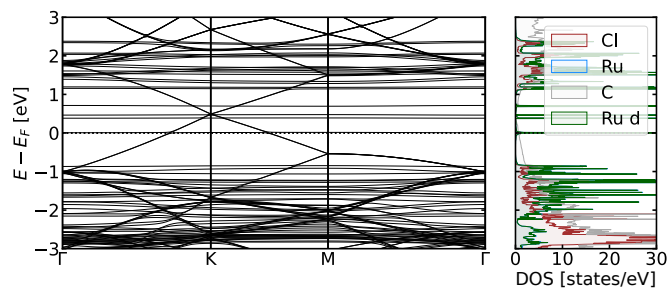
by the green curve, sharply decays within few Angstrom in the perpendicular direction. However, we note a contrast along the chain, where the charge does not order equivalently but has a wave-like behavior (Supplementary Fig. 4c)). The spatially resolved charge transfer increases in value close to the Ru sites with less magnetic moment and decreases close to sites with higher magnetic moment.



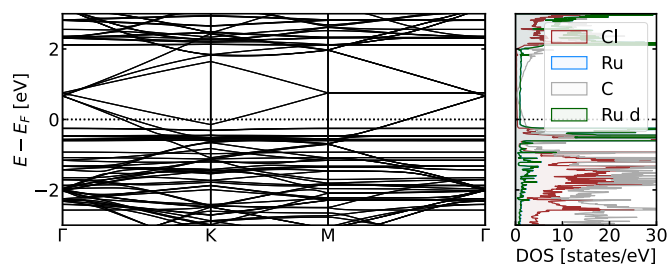
Supplementary Figure 4. Spatial charge redistribution for the tensile strained heterostructure in each direction. Note: the planer average values  $\rho$  are scaled by a factor of 1000.

#### Supplementary Note 5: Electronic properties, extended energy range

In Supplementary Fig. 5 and Supplementary Fig. 6 we show the electronic band structure and atom and orbital resolved density of states (DOS) within increased energy window for the tensile (7.8%) and compressive (-13%) strained structure, respectively. For compressive strained structure within the increased energy window we see the bonding and antibonding formation around -0.5 eV and 2.5 eV due to the Ru-Ru bond shortening.



Supplementary Figure 5. Electronic properties of the relaxed single-chain under tensile strain estimated by DFT+U, with  $U - J = U_{\text{eff}} = 3.0$  eV, in an extended energy window.



Supplementary Figure 6. Electronic properties of the relaxed single-chain under compressive strain estimated by DFT+U, with  $U - J = U_{\text{eff}} = 3.0$  eV, in an extended energy window. We see bonding and anti bonding states for the Ru 4d states, at -0.5 eV and 2.5 eV, respectively.